Characterization of the Electrical Properties of a Double Heterostructure GaN/AlGaN Epitaxial Layer with an AlGaN Interlayer

Meng, Qingzhi[1]; Lin, Qijing[1,2,3,4]; Jing, Weixuan[1]; Mao, Qi[1]; Zhao, Libo[1]; Fang, Xudong[1]; Dong, Tao[4,5]; Jiang, Zhuangde[1,2]

[1]State Key Laboratory of Mechanical Manufacturing Systems Engineering, Xi'an Jiaotong University, China.
[2]Collaborative Innovation Center of High-End Manufacturing Equipment, Xi'an Jiaotong University, China.
[3]School of Mechanical and Manufacturing Engineering, Xiamen Institute of Technology, China.
[4]Chongqing Technology and Business University, China.
[5]Department of Microsystems (IMS), Faculty of Technology, Natural Sciences and Maritime Sciences, University of South-Eastern Norway

This version of the article has been accepted for publication, after peer review (when applicable) and is subject to Springer Nature's AM terms of use, but is not the Version of Record and does not reflect post-acceptance improvements, or any corrections. The Version of Record is available online at: https://doi.org/10.1007/s11664-020-08733-3

Meng, Q., Lin, Q., Jing, W., Mao, Q., Zhao, L., Fang, X., Dong, T., & Jiang, Z. (2021). Characterization of the Electrical Properties of a Double Heterostructure GaN/AlGaN Epitaxial Layer with an AlGaN Interlayer. *Journal of Electronic Materials*, *50*(4), 2521-2529. https://doi.org/10.1007/s11664-020-08733-3

© 2021 The Minerals, Metals & Materials Society.

Characterization of the Electrical Properties of a Double Heterostructure GaN/AlGaN Epitaxial Layer with an AlGaN Interlayer

Qingzhi Meng,[1,&] Qijing Lin,[1,2,3,4,&,*] Weixuan Jing[1], Qi Mao[1], LiboZhao,[1] Xudong Fang, [1] Tao Dong,[5] Zhuangde Jiang,[1,2]

[1]State Key Laboratory of Mechanical Manufacturing Systems Engineering, Xi'an Jiaotong University, Xi'an, 710049, China

[2]Collaborative Innovation Center of High-End Manufacturing Equipment, Xi'an Jiaotong University, Xi'an, 710054, China

[3] School of mechanical and manufacturing engineering, Xiamen Institute of Technology, Xiamen, 361021, China

[4]Chongqing Technology and Business University, Nan'an District, Chongqing 400067, China.

[5]Department of Microsystems (IMS), Faculty of Technology, Natural Sciences and Maritime Sciences, University of South-Eastern Norway, Postboks 235, 3603 Kongsberg, Norway.

***Email: xjjingmi@163.com**

&These authors contributed equally to this work, so they should be both considered as co-first authors.

This paper proposes a double-heterostructure (DH) GaN/AlGaN epitaxial layer that contains an AlGaN interlayer. The electrical properties are characterized and compared with conventional single-heterostructure (SH) GaN/AlGaN epitaxial layers. The Hall effect measurement shows that the DH GaN/AlGaN epitaxial layer has a carrier mobility of 1815 $cm^2 \cdot V^{-1} s^{-1}$, which is approximately 20.37% higher than the SH GaN/AlGaN epitaxial layer. The weak-beam dark-field (WBDF) images taken by a transmission electron microscopy (TEM) show that the AlGaN interlayer in the DH GaN/AlGaN epitaxial layer can block dislocations. The full widths at half maximum (FWHM) results show that there is no significant difference in the screw dislocation density between the SH and DH GaN/AlGaN

epitaxial layers. However, the edge dislocation density and the overall internal stress in the DH GaN/AlGaN epitaxial layer are less than those in the SH GaN/AlGaN epitaxial layer. Finally, the physical mechanism of how edge dislocations impact the electrical properties of a DH GaN/AlGaN epitaxial layer is discussed.

Keywords: double heterostructures, electrical properties, electron mobility, physical mechanism, edge dislocations

INTRODUCTION

Recently, GaN/AlGaN heterostructure field-effect transistors (HFETs) have received considerable attention due to their excellent frequency and power characteristics[1-4]. Their extraordinary physical properties, such as high breakdown voltage[5-7], high power[8,9], and high temperature resistance[10,11] allow GaN/AlGaN HFETs to play an important role in microwave and terahertz fields[12-14]. Studies show that the crystal quality of epitaxial layers substantially affects the device performance. For example, epitaxial layers with a high crystal quality can provide a high confinement of carriers in a two-dimensional electron gas (2DEG) channel, which lead to high current density and output power. Various novel epitaxial structures have been proposed to improve crystal quality, because the crystal quality of epitaxial layers determines the upper limit of device performance. Epitaxial structures including the AlN interlayer[15,16], InGaN back-barrier layer[17,18], and graded AlGaN layer[19,20] have been proposed to improve crystal quality. Among these structures, double-heterostructure (DH) GaN/AlGaN HFETs are proven to have better electrical properties than conventional single-heterostructure (SH) GaN/AlGaN HFETs in terms of the current collapse effect, current-carrying capability and carrier confinement characterization[21-24]. In addition, the DH GaN/AlGaN epitaxial layer's structure optimization has been reported. Marleen Van Hove[25] et al. proposed a DH GaN/AlGaN epitaxial structure with multiple AlGaN buffer layers and optimized each layer's thickness. The mobility was 1766 $cm^2\ V^{-1}s^{-1}$ and the electron density was $1.16\times10^{13}/cm^2$, respectively. Yue Hao's group[26] compared different types of DH GaN/AlGaN with composite buffer layer structures and investigated the crystalline characteristics by an atomic force microscope (AFM) and high resolution X-ray diffraction (HRXRD). Afterwards, they manufactured an HFET based on the DH GaN/AlGaN epitaxial layer[27] and found that the DH GaN/AlGaN HFET had better subthreshold characteristics, switching characteristics, drain-induced barrier lowering (DIBL) effects and breakdown characteristics. Experimental results proved that

the device performance can be improved through the optimization of the epitaxial structure. Nevertheless, crystal quality is still an important factor restricting the electrical properties of the epitaxial layer. Novel epitaxial structures need to be designed and optimized to overcome the crystalline defects.

This paper proposes a DH GaN/AlGaN epitaxial layer containing an AlGaN interlayer. The electrical properties are systematically investigated using the TEM, HRXRD, AFM, C-V measurements, and non-contact Hall effect measurements. The results show that the DH GaN/AlGaN epitaxial layer exhibited a better electrical performance than the SH GaN/AlGaN epitaxial layer due to the lower edge dislocation density.

GROWTH OF THE EPITAXIAL LAYERS

Both the SH and DH GaN/AlGaN epitaxial layers were deposited on c-plane sapphire substrates by MOCVD technology. Triethyl gallium (TEGa), trimethyl aluminium (TMAl) and ammonia (NH_3) were used as the sources of Ga, Al and N, respectively. High-purity hydrogen (H_2) was used as the carrier gas. The cross sections of the two epitaxial layers are shown in Figure 1. For the SH GaN/AlGaN epitaxial layer, a 50 nm AlN nucleation layer was deposited on a sapphire substrate at 980°C and 3.33kPa, followed by a 1.5 µm GaN buffer layer, 1 nm AlN spacer, 23 nm $Al_{0.25}Ga_{0.75}N$ barrier layer and 2 nm GaN cap layer deposited at 920°C and 5.33kPa. For the DH GaN/AlGaN epitaxial layer, a 1.5 µm GaN buffer layer and 23 nm$Al_{0.25}Ga_{0.75}N$ interlayer were deposited with the same thickness and conditions as the SH GaN/AlGaN epitaxial layer. Then, a 40 nm GaN channel layer, 1 nm AlN spacer, 23 nm $Al_{0.25}Ga_{0.75}N$ barrier layer and 2 nm GaN cap layer were deposited on the 23 nm $Al_{0.25}Ga_{0.75}N$ interlayer in that order.

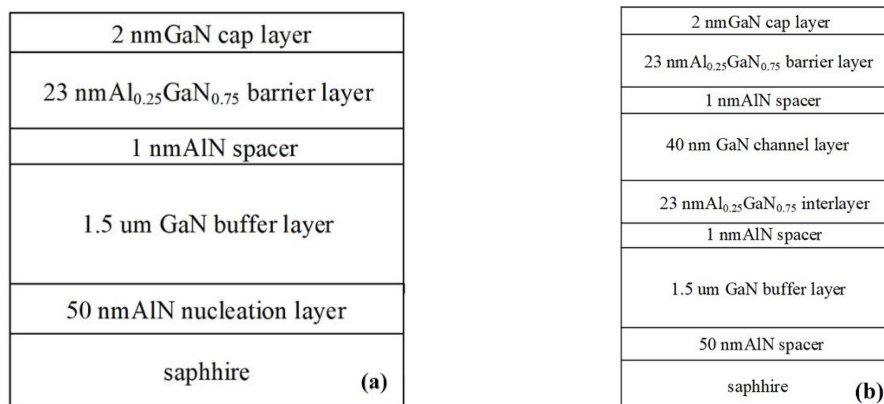

Fig. 1. Diagram of the (a) SH and (b) DH GaN/AlGaN epitaxial layers.

RESULTS AND DISCUSSION

Cross sections of the SH and DH GaN/AlGaN epitaxial layers were observed by TEM (Figure 2). The interface between each layer was clear, and the thickness of each layer was confirmed. The corresponding high-angle annular dark field (HAADF) images are shown in Figure 3. The higher contrast image corresponds to the GaN layer, while the lower contrast image corresponds to the $Al_{0.25}Ga_{0.75}N$ layer. It can be seen that the composition of each layer is uniform with minimal diffusion of Al between the GaN and AlGaN layers. Figure 4 shows the results of EDX line scanning, which displayed the composition of the Al. The calculated Al composition in the barrier layer is 24.3% for the SH GaN/AlGaN epitaxial layer, and the corresponding result of the DH GaN/AlGaN epitaxial layer is 25.4% and 25.1% in the barrier layer and the interlayer, respectively. These results showed that the actual parameters of the epitaxial layers were consistent with the designed structural parameters.

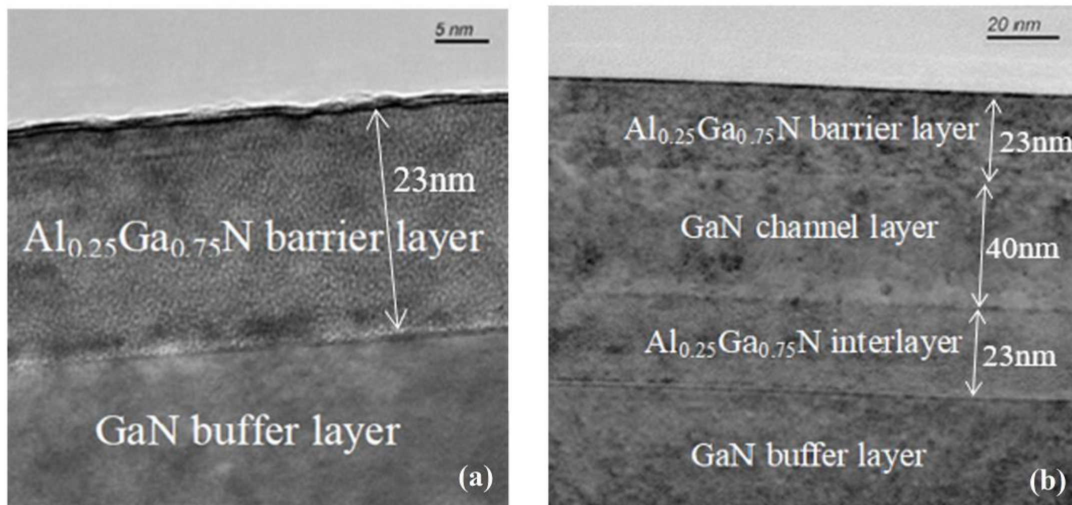

Fig. 2. The TEM image of the cross sections of the **(a)** SH and **(b)** DH GaN/AlGaN epitaxial layers.

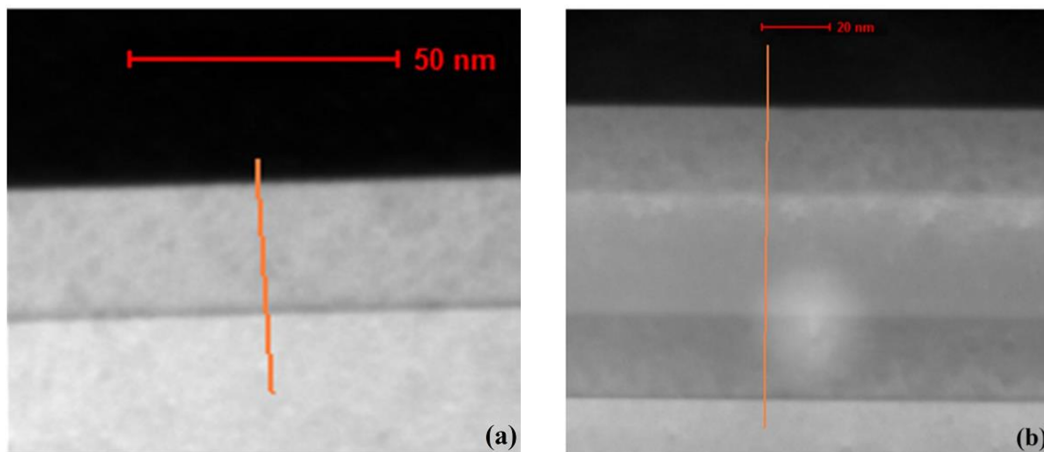

Fig.3. The HAADF image of the **(a)**SH and**(b)** DH GaN/AlGaN epitaxial layers.

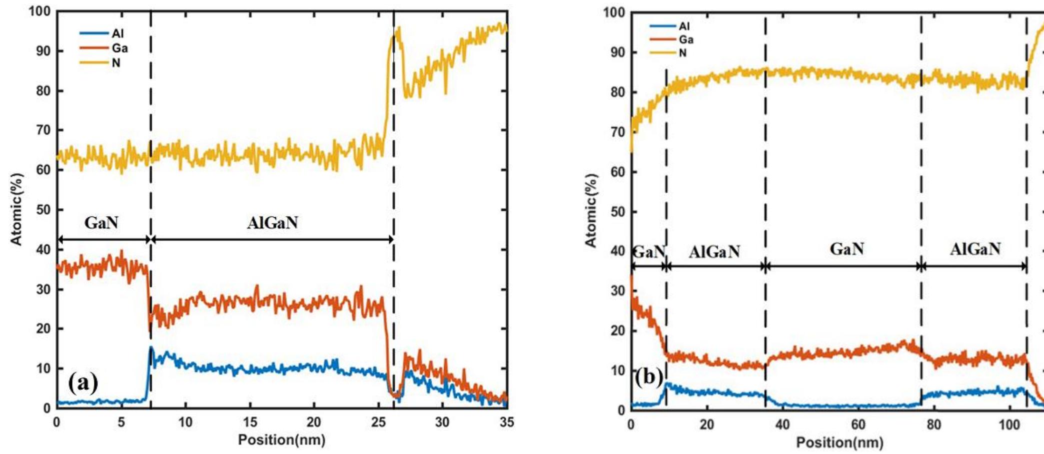

Fig. 4. The EDX line scanned for the **(a)** SH and **(b)** DH GaN/AlGaN epitaxial layers.

The main factor affecting crystal quality is the dislocation defects generated during crystal growth. In the GaN/AlGaN thin film system, the dislocations include screw dislocations, edge dislocations and mixed dislocations. The dislocations were observed by the weak-beam dark-field (WBDF) images. According to the visible-invisible law of dislocations[28], dislocations can not be observed along the **g** direction when **g**·**b**=0 (the diffraction vector g is perpendicular to the Burgers vector b). Thus, the images taken along (0002) and (11-20) showed the screw dislocations (including the component of screw dislocations in the mixed dislocations) and the edge dislocations (including the component of edge dislocations in the mixed dislocations), respectively. So in order to evaluate the distribution of the dislocations in the SH and DH epitaxial layers, the WBDF images were taken along the (0002) and (11-20) directions for SH epitaxial layer (Figure 5) and DH epitaxial layer (Figure 6). Screw dislocations, edge dislocations and mixed dislocations were pointed out with arrows of different colors. In Figure 5(a) and Figure 6(a), there are no significant differences in the amount of screw dislocations between the SH and DH epitaxial layers. In Figure 6(b), the edge dislocations in the DH epitaxial layers are composed of edge dislocations in mixed dislocations and a few pure edge dislocations. The total number of edge dislocations in the DH epitaxial layers is significantly smaller than that of the SH epitaxial layer in Figure 5(b). In addition, a number of edge dislocations in the SH epitaxial layer continue to propagate up to the

surface layer. However, in the DH epitaxial layer, a number of edge dislocations terminate either at the bottom or beyond the bottom of the GaN/AlGaN interface. Only a few dislocations reach the surface of the layer. This indicates that the insertion of the AlGaN interlayer decreases the number of dislocations. This also indicates the AlGaN interlayer blocks or changes the propagation direction of dislocation lines, which increases the probability of the annihilation and termination of dislocations[29-31]. However, the insertion of the AlGaN interlayer changed the stress distribution of nearby layers, which may generate new dislocations. To evaluate the influence of the AlGaN interlayer on the dislocation density, the coupled effect of blocking dislocations and generating new dislocations needs to be analysed. When the inserted AlGaN interlayer exceeds the critical thickness of elastic relaxation, the $Al_{0.25}GaN$ turns to be plastic relaxed. Thus the tensile stress is strong enough to change the direction of dislocations propagation, causing them to meet, react, and annihilate[31]. The introduction of the $Al_{0.25}GaN$ interlayer may generate non-significant new dislocations, because the lattice mismatch between GaN and $Al_{0.25}GaN$ is small. Therefore, the intercalation layer plays a positive role in reducing dislocations. In the DH structure, most dislocations were blocked below the GaN/AlGaN interface, and only a small number of dislocations were newly generated, so one may make the prediction that the AlGaN interlayer contributes to the reduction of crystal dislocations. Through the TEM observations, we were able to analyze the distribution of crystal dislocations only semi-quantitatively. In order to further investigate the accurate dislocation density and the effect on the electrical properties of the epitaxial layers, more characterization studies need to be carried out.

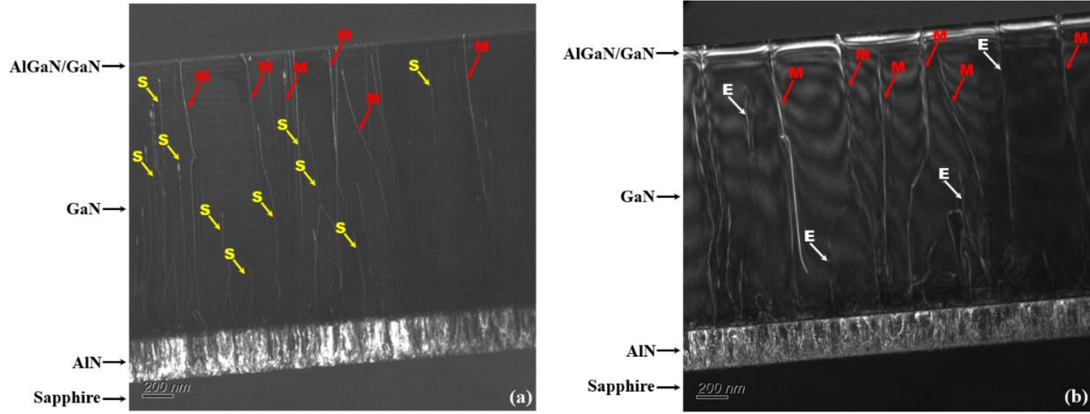

Fig. 5. The WBDF images of SH GaN/AlGaN epitaxial layer taken by TEM alone (a) (0002) and (b) (11-20) direction. The yellow arrows refer to pure screw dislocations, the white arrows refer to pure edge dislocations, and the red arrows refer to mixed dislocations.

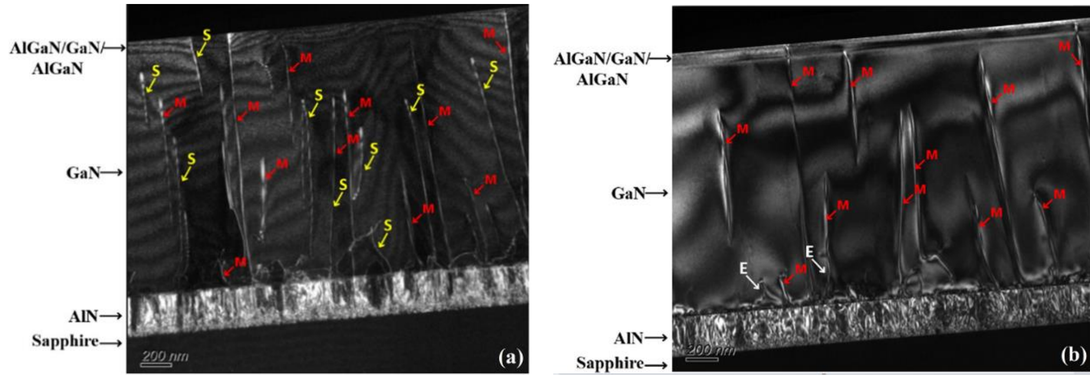

Fig. 6. The WBDF images of DH GaN/AlGaN epitaxial layer taken by TEM alone(a) (0002) and (b) (11-20) direction. The yellow arrows refer to pure screw dislocations, the white arrows refer to pure edge dislocations, and the red arrows refer to mixed dislocations.

The FWHM of the rocking curves for the (002) and (102) directions of the epitaxial layers were measured by HRXRD, as these two vectors are sensitive to screw dislocations and edge dislocations. The (002) FWHMs of the GaN buffer layer for the SH and DH GaN/AlGaN epitaxial layers are 617 arcsec and 605 arcsec, respectively. As shown in Figure 7, The (102) FWHMs of the SH and DH epitaxial layers are 1950 arcsec and 1242 arcsec, respectively. The relationship between the dislocations and FWHM can be expressed as

$$D = \frac{\beta^2}{4.35b^2} \tag{1}$$

where D is the dislocation density, β is the measured FWHM, and b is the length of the Burgers vector. The calculation results of the screw dislocation density are $3.51\times10^8/cm^2$ and $3.18\times10^8/cm^2$ for the SH

and DH GaN/AlGaN epitaxial layer, respectively. The edge dislocation density of SH and DH GaN/AlGaN epitaxial layer are $3.65\times10^9/cm^2$ and $1.48\times10^9/cm^2$, respectively. The screw dislocation density in the DH GaN/AlGaN is slightly lower than that in the SH GaN/AlGaN epitaxial layer, while the edge dislocation density is much lower in the DH GaN/AlGaN layer. These results are consistent with the TEM observations in Figure 5 and 6. The dislocations in the crystal were mainly generated during the deposition of the thin films. These dislocations will induce a stress field between crystal planes, leading to a variation in the crystalline interplanar spacing and a shift of the diffraction peak. The vertical distance of the adjacent crystal planes can be calculated by the Bragg equation:

$$d = \frac{n\lambda}{2sin\theta} \tag{2}$$

where λ is the wavelength of the X-ray on the crystal, θ is the incidence and reflection angle of the X-ray , and n is the order of the reflected beam. The stress in the films can be expressed as

$$\sigma = \frac{-E(d - d_0)}{2vd_0} \tag{3}$$

where E is Young's modulus of the film, v is Poisson's ratio, and $d_0$is the distance between the adjacent crystal planes without stress. In the experiment, the wavelength of the X-ray (CuKa) is λ=0.154056 nm, the Young's modulus of the GaN film is E=293 GPa[33], and the Poisson's ratio of the GaN is v= 0.183[34]. The calculated stresses of the (002) and (102) planes in the SH GaN crystal are 0.20 GPa and 9.91 GPa, respectively. The stresses in the corresponding DH are 0.12 GPa and 8.60 GPa. The stresses in the DH epitaxial layer of the (002) and (102) planes are less than that in the SH epitaxial layer. The screw dislocations and edge dislocations will cause a variation in the spacing of the (002) and (102) planes. Hence, a lower dislocation density corresponds to a smaller stress field.

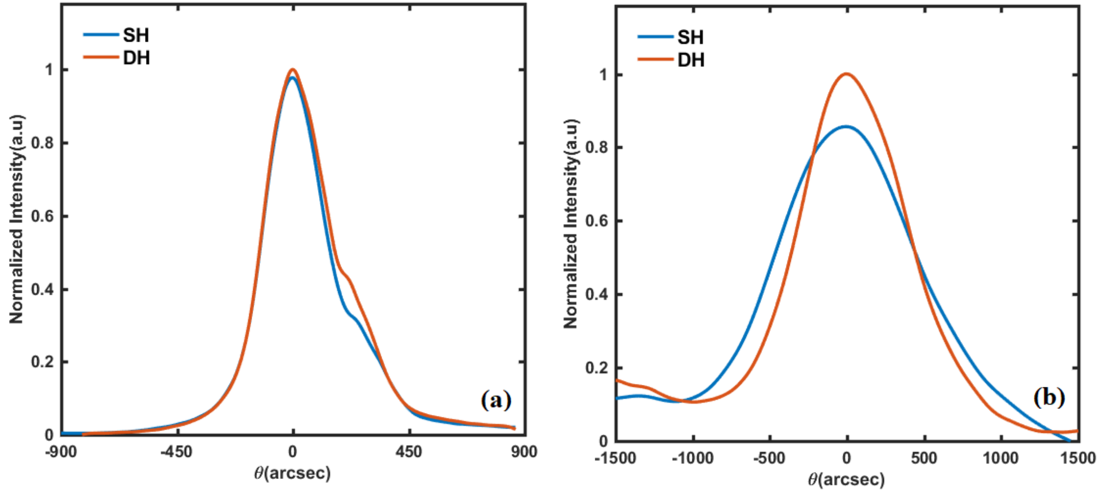

Fig. 7. The XRD results: (a) (002) and (b) (102) rocking curves of the SH and DH epitaxial layers.

Figure 8 shows the surface morphology of the SH and DH GaN/AlGaN epitaxial layers scanned by AFM with an area of 5×5 μm^2. The root mean square (RMS) values of the SH and DH GaN/AlGaN epitaxial layers are 0.402 nm and 0.538 nm, respectively. Both layers show low surface roughness. Due to the insertion of the AlGaN interlayer in the DH epitaxial layer, there was a slight fluctuation in the bottom GaN/AlGaN interface and the surface, but the overall performance was not significantly influenced.

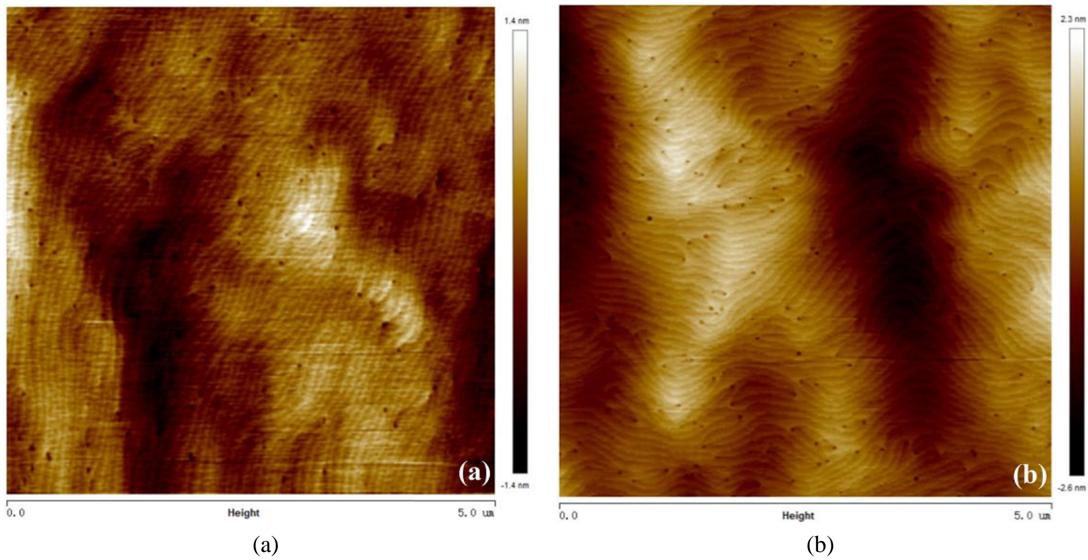

(a) (b)

Fig. 8. Surface roughness of the (a) SH and (b) DH epitaxial layers scanned by the AFM.

The electrical properties of the SH and DH GaN/AlGaN epitaxial layers were measured by a C-V tester and the non-contact Hall effect measurement system. Figure 9 shows the C-V characteristics of the SH and DH GaN/AlGaN epitaxial layers. Both epitaxial layers show good confinement of the 2DEG without parasitical capacitances. The longitudinal distribution of the carrier concentration in epitaxial

layers and the sheet density of the 2DEG can be extracted from the C-V curve. The carrier concentration N is expressed as

$$N = \frac{C^3}{q\varepsilon\varepsilon_0 A^2}\frac{dV}{dC} \tag{4}$$

$$C = \frac{\varepsilon\varepsilon_0 A}{z} \tag{5}$$

where ε=9.5 is the relative dielectric constant of AlGaN, ε_0=8.854×10^{-14} C/V·cm is the permittivity of the vacuum, A is the contact area between the probe and the epitaxial layer surface, and z is the depth of the depletion region. The distributions of carrier concentration in the SH and DH epitaxial layers are shown in Figure 10. The sheet density of the 2DEG is then calculated as

$$n_s = \int_0^\infty N(z)\,dz \tag{6}$$

The sheet densities of the SH and DH GaN/AlGaN epitaxial layers are 1.019×10^{13}/cm^2 and 8.247×10^{12}/cm^2, respectively.

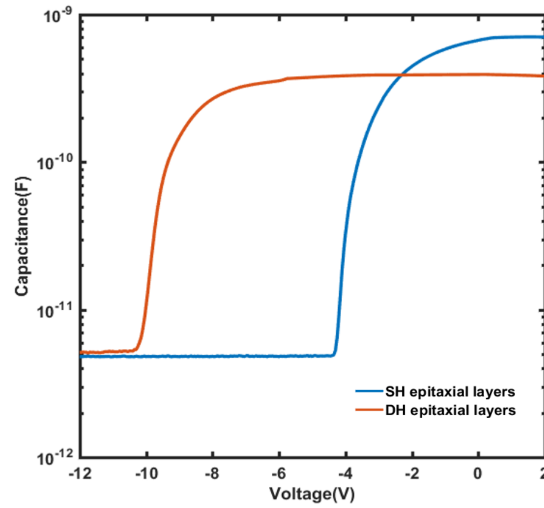

Fig. 9. The C-V characteristics of the SH and DH GaN/AlGaN epitaxial layers.

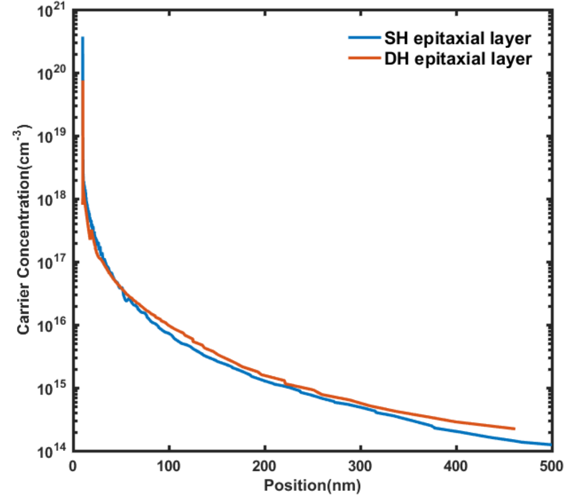

Fig. 10. The distributions of carrier concentration in the SH and DH GaN/AlGaN epitaxial layers.

The electron mobility and sheet resistance were tested by the non-contact Hall measurement system. The average mobilities of the SH and DH GaN/AlGaN epitaxial layers are 1508cm^2/V·s^{-1} and 1815cm^2/V-s, respectively. The result of the DH layer is approximately 20.37% higher than that of the SH layer with the same structural parameters. The average sheet resistances of SH and DH GaN/AlGaN are 357.75 Ω/□ and 348.65 Ω/□, respectively. All the measured material parameters and electrical properties of the SH and DH GaN/AlGaN epitaxial layers are summarized in Table 1.These results show that the DH epitaxial layer has better electron transport capacity and 2DEG confinement ability than SH epitaxial layer. One may make the prediction that in DH GaN/AlGaN HEMT, a better DC characteristic and higher breakdown voltage could be owned, which are beneficial for the application of RF and high power devices. Future studies may verify this prediction through the future preparation of DH GaN/AlGaN HEMTs and the DC measurement.

Table I. The measured material parameters and electrical properties of the SH and DH epitaxial layers

	Screw dislocations [cm^{-3}]	Edge dislocations [cm^{-3}]	Stress (002) [GPa]	Stress (102) [GPa]	RMS [nm]	Sheet carrier density [cm^{-2}]	Mobility [cm^2·V^{-1}s^{-1}]	Sheet resistance [Ω/□]
SH	3.51×10^8	3.65×10^9	0.20	9.91	0.402	1.019×10^{13}	1508	357.75
DH	3.18×10^8	1.48×10^9	0.12	8.60	0.538	8.247×10^{12}	1815	348.65

As shown in Table I, there is a significant difference in the edge dislocation density between the SH and DH structures. Moreover, the electrical properties and other parameters are related to dislocations in the crystal. Therefore, edge dislocations in the GaN/AlGaN film system, rather than screw dislocations, are the dominant factors affecting the electrical properties. This is because the edge dislocations can generate acceptor centres and capture electrons from the conduction band. Thus, the free electron concentration will reduce significantly near the edge dislocations. The lattice expansion caused

by free electrons will be weakened, and the distance of the adjacent crystal planes will be reduced. Therefore, a stress field is created around the edge dislocations. In the DH GaN/AlGaN epitaxial layer, the edge dislocation density is less than that of the SH GaN/AlGaN epitaxial layer with the introduction of the AlGaN interlayer, resulting in a reduction in the overall stress and a shrinkage of the GaN bandgap[35], as shown in Figure 11. The shrinkage of the bandgap is accompanied by a decrease in the triangular barrier, leading to a weaker confinement of the 2DEG in the channel. Although the sheet carrier density is larger in the SH epitaxial layer than in the DH epitaxial layer, dislocations penetrating the interface will exert an obvious influence on the degradation of electrical properties in GaN HFETs. This is because the 2DEG is formed at the interface of the GaN/AlGaN layer. This can be explained by Matthiessen's rule[36]. The five scattering parameters that affect the carrier mobility are the polar optical phonons parameter μ_{OP}, dislocation parameter μ_{DIS}, interface roughness parameter μ_{IR}, acoustic phonon parameter μ_{AP}, and ionized impurity parameter μ_{II}. The total carrier mobility is expressed as

$$\frac{1}{\mu_{tot}} = \frac{1}{\mu_{OP}} + \frac{1}{\mu_{DIS}} + \frac{1}{\mu_{IR}} + \frac{1}{\mu_{AP}} + \frac{1}{\mu_{II}} \tag{7}$$

The rate of alloy disorder scattering is small and negligible[36] with the 1 nm AlN layer. The ionized impurity scattering in SH and DH GaN/AlGaNGaN/AlGaN epitaxial layers are similar because both epitaxial layers were unintentionally doped. In equation (7), the total carrier mobility mainly depends on the dislocations and the interface roughness. As the edge dislocation density is lower in the DH GaN/AlGaN epitaxial structure than in the SH GaN/AlGaN epitaxial structure, the probability of dislocation scattering in the 2DEG channel is also lower. On the other hand, the TEM and AFM results show that the DH epitaxial layer has a smoother interface because the dislocation lines propagating from the GaN buffer layer are blocked by the AlGaN interlayer. The comprehensive effect of edge dislocation density and interface roughness causes higher electron mobility in the DH GaN/AlGaN epitaxial layer.

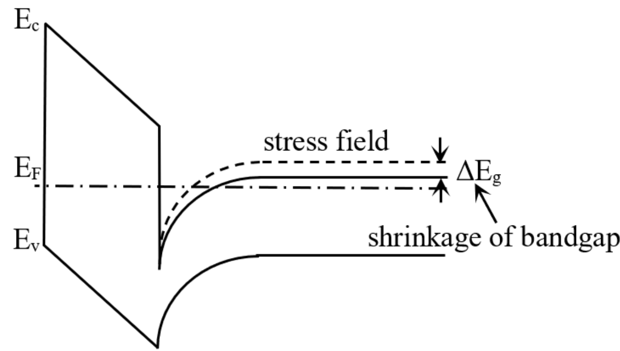

Fig. 11. Schematic diagram of bandgap shrinkage.

CONCLUSIONS

In this paper, a DH GaN/AlGaN epitaxial layer with an AlGaN interlayer is proposed and prepared. The electrical properties are systematically studied and compared with a SH GaN/AlGaN epitaxial layer. The TEM images show that the prepared epitaxial layers are consistent with the designed structural parameters. The WBDF and HRXRD results show that the edge dislocation density in the DH epitaxial layer is much lower than that in the SH GaN/AlGaN epitaxial layer due to insertion of the AlGaN interlayer. The electrical properties are measured by a C-V tester and non-contact Hall effect measurement system, and a carrier mobility of 1815 $cm^{2}\cdot V^{-1}s^{-1}$ is obtained, which is 20.37% higher than that of the SH GaN/AlGaN structure. In addition, the mechanism of edge dislocations affecting the electrical properties is explained by energy band theory and Matthiessen’s rule.

ACKNOWLEDGMENTS

The authors would like to thank the financial support from the National Natural Science Foundation of China (No. 51890884, No. 91748207, No. 51805421), and the China Postdoctoral Science Foundation (No. 2018T111045). We also appreciated the support from the International Joint Laboratory, Key Laboratory of Wide Band Gap Semiconductor Materials and Devices, and Sinoma Institute of Materials Research (Guang Zhou) Co., Ltd for Micro/Nano Manufacturing and Measurement Technologies.

STATEMENT

The authors declare that they have no conflict of interest.

REFERENCES

[1] H. Wu, B. X. Duan, L. Y. Yang, Y. T. Yang, Chin. Phys. B. 28, 027302 (2019).

[2] X. Y. Zhou, X. Tan, Y. J. Lv, Y. G. Wang, X. B. Song, G. D. Gu, P. Xu, H. Y. Guo, Z. H. Feng, S. J. Cai, IEEE Trans. Electron Devices. 65, 928 (2018).

[3] M. Charles, Y. Baines, R. Bouis, A. M. Papon, Phys. Status Solidi B-Basic Solid State Phys. 255, 1700406 (2018).

[4] A. S. Augustine Fletcher, D. Nirmal, Superlattices Microstruct. 109, 519(2017).

[5] M. Tao, S.F. Liu, B. Xie, C. P. Wen, J. Y. Wang, Y. L. Hao, W. G. Wu, K. Cheng, B. Shen, M. J. Wang, IEEE Trans. Electron Devices. 65, 1453 (2018).

[6] Y. Li, G. I. Ng, S. Arulkumaran, Z. H. Liu, K. Ranjan, W. C. Xing, K. S. Ang, P. P. Murmu, J. Kennedy, Phys. Status Solidi A-Appl. Mat.214, 1600555 (2017).

[7] J. F. Du, Z. G. Jiang, Z. Y. Bai, P. L. Pan, Q. Yu, J. Comput. Electron. 16, 748 (2017).

[8] M. Forouzanfar, M. Joodaki, AEU-Int. J. Electron. Commun.84, 225 (2017).

[9] Y. K. Sin, J. Bonsall, Z. Lingley, M. Brodie, M. Mason, in *Conference on Gallium Nitride Materials and Devices XII* (2017), 10104.

[10] G. Pavlidis, D. Kendig, ER. Heller,S. Graham, IEEE Trans. Electron Devices.65, 1753 (2018).

[11] S. K. Tsung, D. Y. Lin, C. F. Lin, C. W. Chang, J. C. Zhang, S. J. Tu, J. Cryst. Growth. 464, 175 (2016).

[12] C. Daher, J. Torres, I. Iniguez-De-La-Torre,P. Nouvel, L. Varani, P. Sangare, G. Ducournau, C. Gaquiere, J. Mateos, T. Gonzalez, IEEE Trans. Electron Devices.63, 353 (2016).

[13] Z. F. Tian, P. Xu, Y. Yu, J. D. Sun, W. Feng, Q. F. Ding, Z. W. Meng, X. Li, J. H. Cui, Z. X. Zheng, X. X. Li, L. Jin, H. Qin, Y. F. Sun,Chin. Phys. B.28, 359 (2019).

[14] X. Li, J. D. Sun, H. J. Huang, Z. P. Zhang,L. Jin, Y. F. Sun, V. V. Popov, H. Qin, Chin. Phys. B.28, 118502 (2019).

[15] C. Liu, A. Kumamoto, H. Sodabanlu, M. Sugiyama, Y. Nakano, in *10th International Conference on Nitride Semiconductors* (*ICNS*) (2013), p. 147.

[16] J. Liu, J. Zhang, Q. Mao, X. Wu, F. Jiang, Crystengcomm.15, 3372 (2013).

[17] Y. Bi, X. L. Wang, H. L. Xiao, C. M. Wang, E. C. Peng, D. F. Liu, C. Feng, L. J. Jiang, Eur. Phys. J.-Appl. Phys. 55,10102 (2011).

[18] G. G. Liu, K. Wei, J. Huang, X. Y. Liu, J. B. Niu, J. Infrared Millim. Waves. 30, 289 (2012).

[19] B. Leung, J. Han, Q. Sun, Phys. Status Solidi C, 11, 437 (2014).

[20] Y. A. Chang, J. Y. Chang, Y. T. Kuo, Y. T. Kuo, Y. K. Kou, Appl. Phys. Lett,100, 251102 (2012).

[21] R. Gaska, MS. Shur, TA. Fjeldly,A. D. Bykhovski, Appl. Phys. Lett. 85, 3009(1999).

[22] RM. Chu, YG. Zhou, J. Liu,DL. Wang, KJ. Chen, KM. Lau, IEEE Trans. Electron Devices. 52, 438 (2005).

[23] A. Vescan, H. Hardtdegen, N. Ketteniss, M. Eickelkamp, A. Noculak, J. Goliasch, M. Vonder Ahe, HL. Bay, T. Schapers, H. Kalisch, D. Grutzmacher, RH. Jansen, Phys. Status Solidi C. 6, S1003 (2009).

[24] J. Y. Zheng, J. S.Wu, D. Y. Lin, H. J.Lin, Phys. Status Solidi C, 6, 1944(2008).

[25] K. Cheng, H. Liang, M. Van Hove, K. Geens, B. D. Jaeger, P. Srivastava, X. W. Kang, P. Favia, H. Bender, S. Decoutere, J. Dekoster, J. I. Del Agua Borniquel, S. W. Jun, H. Chung, Appl. Phys. Express. 5, 011002(2012).

[26] F. N. Meng, J. C. Zhang, H. Zhou, J. C. Ma, J. S. Xue, L. S. Dang, L. X. Zhang, M. Lu, S. Ai, X. G. Li, Y. Hao, J. Appl. Phys.112, 023707 (2012).

[27] W. H. Zhang, X. D. Li, J. C. Zhang, H. Q. Jiang, X. Xu, Z. X. Guo, R. Y. Jiang, Z. Yu, Y. L. He, Y. Hao, Phys. Status Solidi A-Appl. Mat. 213, 2203 (2016).

[28] N. Kuwano, T. Tsuruda, Y. Adachi,S. Terao, S. Kamiyama, H. Amano, I. Akasaki,Phys. Status Solidi A-Appl. Mat.192, 366 (2002).
[29] L. W. Sang, Z. X. Qin, H. Fang,T. Dai, Z. J. Yang, B. Shen, G. Y.Zhang, X. P. Zhang, J. Xu, D. P. Yu,Appl. Phys. Lett. 93, 103 (2008).
[30] H. H. Sun, F. Y. Guo, D. Y. Li, L. Wang, D. G. Zhao, L. C. Zhao, Chin. Phys. Lett. 29, 096101 (2012).
[31] H. H. Sun, F. Y. Guo, D. Y. Li, L. Wang, D. B. Wang, L. C. Zhao, Nanoscale Res. Lett. 7, 1 (2012).
[32] J. N. Lv, Z. C. Yang, G. Z. Yan, Y. Cai, B. S. Zhang, K. J. Chen, in *24th IEEE International Conference on Micro Electro Mechanical Systems* (*MEMS*) (2011), 388.
[33] J. Tweedie, R. Collazo, A. Rice, J. Q. Xie, S. Mita, R. Dalmau, Z. Sitar, J. Appl. Phys.108, 043526 (2010).
[34] Z. Y. Gao, Y. Hao, J. C. Zhang, P. X. Li, W. P. Gu, Chin. Phys. B.18, 4970 (2009).
[35]E. C. Peng, X. L. Wang, H. L. Xiao, C. M. Wang, H. B. Yin, H. Chen, C. Feng, L. J. Jiang, X. Hou, Z. G. Wang,J. Cryst. Growth. 383, 25 (2013).